*Sādhanā* Vol. 41, No. 2, February 2016, pp. 125–145 



# Modelling and analysis of an open-loop induction motor drive incorporating the effect of inverter dead-time

ANIRUDH GUHA* and G NARAYANAN

Department of Electrical Engineering, Indian Institute of Science,
Bengaluru 560 012, India
e-mail: aguha@ee.iisc.ernet.in; gnar@ee.iisc.ernet.in

MS received 19 November 2014; revised 1 September 2015; accepted 26 September 2015

**Abstract.** The objective of this paper is to study the influence of inverter dead-time on steady as well as dynamic operation of an open-loop induction motor drive fed from a voltage source inverter (VSI). Towards this goal, this paper presents a systematic derivation of a dynamic model for an inverter-fed induction motor, incorporating the effect of inverter dead-time, in the synchronously revolving dq reference frame. Simulation results based on this dynamic model bring out the impact of inverter dead-time on both the transient response and steady-state operation of the motor drive. For the purpose of steady-state analysis, the dynamic model of the motor drive is used to derive a steady-state model, which is found to be non-linear. The steady-state model shows that the impact of dead-time can be seen as an additional resistance in the stator circuit, whose value depends on the stator current. Towards precise evaluation of this dead-time equivalent resistance, an analytical expression is proposed for the same in terms of inverter dead-time, switching frequency, modulation index and load impedance. The notion of dead-time equivalent resistance is shown to simplify the solution of the non-linear steady-state model. The analytically evaluated steady-state solutions are validated through numerical simulations and experiments.

**Keywords.** Dead-time; dynamic model of induction motor; induction motor drive; voltage source inverter; space vector; synchronous reference frame; variable speed drive.

## 1. Introduction

The switches in a power electronic converter are, oftentimes, assumed to be ideal. Ideal switches have zero on-state drop and off-state leakage current; these switch instantaneously between the on and off states. However, in practical switches, the on-state forward drop is significant, and leads to conduction losses. Also, the switching transitions are not instantaneous, leading to switching losses. Both losses result in heating of the device.

A three-phase voltage source inverter, shown in figure 1, consists of three legs with two switches per leg. The forward drop causes a reduction in the ac side terminal voltage, but this is negligible when the dc bus voltage $V_{dc}$ is much greater than the forward voltage drop. The switching transitions being non-instantaneous, there exists a possibility of a shoot-through fault during commutation on account of the over-lapping conduction periods of the two switches in a VSI leg. Hence, a short dead-time duration is introduced, during which the gating pulses of both the top and bottom switches are maintained low. The main objective of this paper is to study the impact of this inverter dead-time on the steady as well as dynamic behaviour of a VSI fed induction motor drive.

The inverter dead-time is known to result in an error voltage pulse in each carrier cycle (details are given in section 3). The width of the error voltage pulse is equal to the dead-time; its magnitude is equal to the dc bus voltage $V_{dc}$; its sign or polarity depends on the direction of the phase current [1, 2]. The cumulative effect of these short-duration pulses over a fundamental cycle includes low-frequency harmonics in the inverter output and also certain change in the fundamental voltage [1–4]. The change in fundamental voltage is important from the control perspective, and can be modelled as a drop across a fictitious "equivalent" resistance [5–8]. This paper presents an analytical expression for this dead-time equivalent resistance. The validity of this expression is established by first using this to predict the steady-state performance of the motor drive, which is then confirmed by simulation and experimental results.

While the effects of inverter dead-time in terms of low-frequency distortion and change in fundamental voltage are reasonably straightforward to see [1–4], the dead-time is also found to impact the stability of the motor drive [5–7, 9–13]. It is reported in [9] that variable speed induction motors could be inherently unstable at low and medium speeds, and particularly under light load conditions. This

*For correspondence

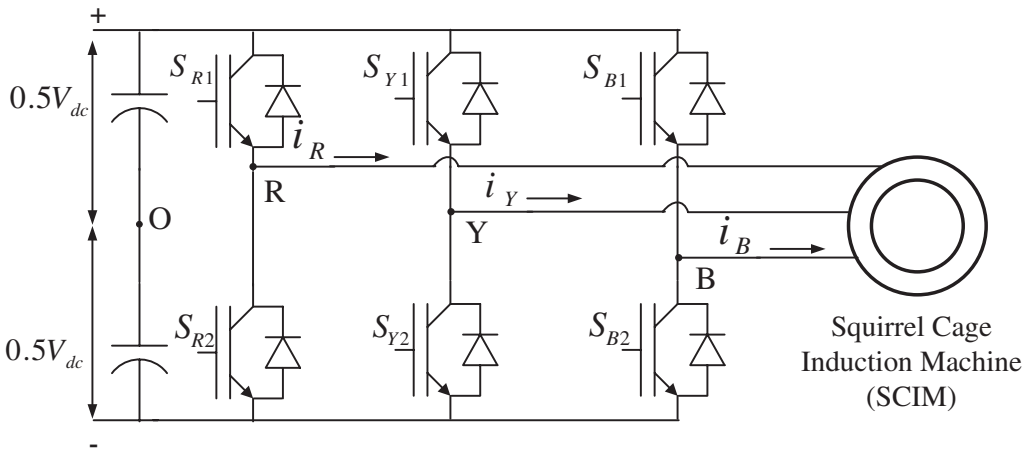


**Figure 1.** Voltage-source inverter fed three-phase induction motor drive [6].

instability in motors is accentuated on account of inverter dead-time. Oscillations in the motor current, torque and speed of constant volts-per-hertz induction motor drive are demonstrated experimentally at low and medium speeds under light load conditions [10]. This experimental study is reported on induction motors rated 3.3kW, 5.5kW and 11kW, considering different values of inverter dead-time [10]. It is suggested that the inverter dead-time could be viewed as an additional stator resistance, leading to instability and oscillatory behaviour of the induction motor [5, 11]. Small-signal stability analyses and experiments that demonstrate instability in 7.5kW, 11kW and 22kW induction motors are presented in [7]. More recently, an experimental study on dead-time induced oscillations in a practical 100-kW induction motor drive is reported in [6]. The stability analysis of this 100-kW induction motor fed from an inverter with significant dead-time is presented in Guha & Narayanan [13, 14]

In [13], small-signal stability analysis is used to predict oscillatory behaviour of the 100-kW motor drive in certain operating regions, which is then confirmed through simulation and experimental results. For stability analysis, certain dynamic model of the induction motor is employed [13], which is different from the standard motor model [15]. This dynamic model includes the dead-time effect by means of a non-linear resistive drop term in the stator voltage equations. However, the derivation of this model is not presented in [13]. This improved dynamic model is derived systematically in the present paper.

Further, small-signal analysis involves perturbation of the system about an equilibrium point. Determination of the equilibrium point of the motor drive involves steady-state solution of its dynamic model. To the best of authors' knowledge, the steady-state solution of the improved dynamic model in [13] or any comparable dynamic model has not been discussed in the literature. Such steady-state solution is not quite straightforward as discussed in section 5 of this paper.

The improved dynamic model of the induction motor and its steady-state solution are important from the point of view of transient analysis and steady-state analysis, respectively, of a practical motor drive. The importance and relevance of these two are not limited to small-signal stability analysis alone. While the oscillatory behaviour on account of dead-time could be limited to a fraction of motor drives and certain operating conditions, the inverter dead-time itself is universal in all inverter-fed motor drives. Hence, the objective of this paper is to study the impact of dead-time on the steady and transient behaviour of the motor drive.

The improved dynamic model is derived here and is used to simulate the steady-state and transient behaviour of the induction motor drive. The dynamic model is further used to derive the steady-state model, which turns out to be non-linear. The solution of the steady-state model is quite involved and requires an iterative procedure. A simplified procedure for the steady-state solution is presented here. This simplified procedure includes analytical evaluation of the dead-time equivalent resistance ($R_{eq0}$). The impact of dead-time on the steady-state operating conditions is brought out by analysis, and is well supported by simulation and experimental results.

## 2. Induction motor dynamic equations in the synchronous reference frame

Figure 2 indicates the axes of the three-phase windings (R, Y, B) of an induction motor. The q-axis and d-axis of the synchronous reference frame revolve at the synchronous angular frequency $\omega_s$ as indicated in the figure. The q-axis is aligned with the stator voltage vector. The q-axis leads the d-axis by 90°; the reference frame angle $\theta$ is measured from the R-phase axis to the q-axis in the counter clockwise sense. The transformation of the three-phase stator voltages

($v_{RN}$, $v_{YN}$, $v_{BN}$) to the q-axis and d-axis voltages (i.e. $v_{qs}$ and $v_{ds}$) is given as follows:

$$\begin{bmatrix} v_{qs} \\ v_{ds} \end{bmatrix} = \frac{2}{3} \begin{bmatrix} \cos(\theta) & \cos(\theta - 120°) & \cos(\theta - 240°) \\ \sin(\theta) & \sin(\theta - 120°) & \sin(\theta - 240°) \end{bmatrix} \begin{bmatrix} v_{RN} \\ v_{YN} \\ v_{BN} \end{bmatrix}. \quad (1)$$

Other three-phase quantities such as motor currents are also transformed in a similar fashion. The transformation angle $\theta$ is given by the following equation

$$\theta = \int \omega_s dt - 90°. \quad (2)$$

The dynamic equations of the induction machine in the synchronously revolving dq frame are given as below [15]:

$$v_{qs} = \left(r_s + L_s \frac{d}{dt}\right) i_{qs} + \omega_s L_s i_{ds} + L_m \frac{di'_{qr}}{dt} + \omega_s L_m i'_{dr} \quad (3)$$

$$v_{ds} = -\omega_s L_s i_{qs} + \left(r_s + L_s \frac{d}{dt}\right) i_{ds} - \omega_s L_m i'_{qr} + L_m \frac{di'_{dr}}{dt} \quad (4)$$

$$\begin{aligned} v'_{qr} &= 0 = L_m \frac{di_{qs}}{dt} + (\omega_s - \omega_r) L_m i_{ds} + \left(r'_r + L'_r \frac{d}{dt}\right) i'_{qr} \\ &+ (\omega_s - \omega_r) L'_r i'_{dr} \end{aligned} \quad (5)$$

$$\begin{aligned} v'_{dr} &= 0 = -(\omega_s - \omega_r) L_m i_{qs} + L_m \frac{di_{ds}}{dt} - (\omega_s - \omega_r) L'_r i'_{qr} \\ &+ \left(r'_r + L'_r \frac{d}{dt}\right) i'_{dr} \end{aligned} \quad (6)$$

$$T_e = T_l + \left(\frac{2}{poles}\right) J \frac{d\omega_r}{dt} + \left(\frac{2}{poles}\right) B\omega_r, \quad (7)$$

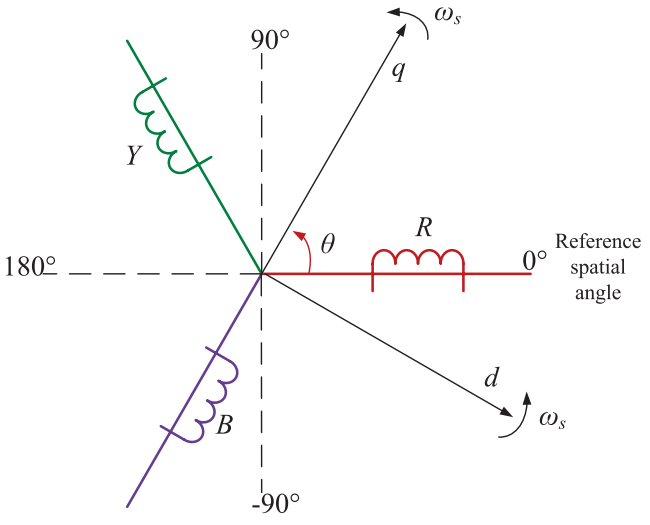


**Figure 2.** Synchronous reference frame transformation [16].

where the electromagnetic torque $T_e$ is given by

$$T_e = \frac{3}{2} \left(\frac{poles}{2}\right) L_m (i_{qs} i'_{dr} - i_{ds} i'_{qr}). \quad (8)$$

The stator q-axis current $i_{qs}$, the stator d-axis current $i_{ds}$, the rotor q-axis current (referred to the stator side) $i'_{qr}$, the rotor d-axis current (referred to the stator side) $i'_{dr}$ and the rotor electrical speed $\omega_r$ form a good choice of state variables that represent the induction motor model. The q-axis stator voltage ($v_{qs}$) and d-axis stator voltage ($v_{ds}$) are considered as system inputs. The synchronous speed $\omega_s$ relates to the frequency of the applied stator voltage. The load torque $T_l$ is another system input. The q- and d-axes rotor voltages (i.e. $v'_{qr}$ and $v'_{dr}$) are zero for a squirrel-cage rotor. The electrical parameters are the stator resistance of the motor $r_s$, and the rotor resistance (referred to the stator side) $r'_r$, the stator inductance $L_s$, the rotor inductance (referred to the stator side) $L_{r'}$, and the mutual inductance $L_m$. The mechanical parameters of the model are inertia $J$ and the friction coefficient $B$.

The above equations constitute a dynamic model of an induction motor, ignoring inverter dead-time. In order to incorporate the effect of inverter dead-time in the dynamic equations of an inverter fed induction motor, the dead-time effect is first reviewed in the following section.

## 3. Effect of dead-time on the inverter output voltage

The effect of dead-time on the inverter output voltage is reviewed in this section. The error voltage on account of dead-time is transformed into and analysed in the space vector domain [8, 16].

### 3.1 *Instantaneous and average error in inverter output voltage*

For safe commutation between the top and bottom switches in an inverter leg (see figure 1), the rising edges of the ideal gating signals $S_{R1}$ and $S_{R2}$, are delayed by dead-time $t_d$ to obtain the actual gating signals $S_{R1d}$ and $S_{R2d}$ as shown in figure 3(a). As seen, both the gating signals $S_{R1d}$ and $S_{R2d}$ are low during the dead-time interval, and one of the two diodes conducts during this interval. The load current polarity determines if the top or bottom diode conducts. This, in-turn, determines the pole voltage during the dead-time interval. For a bottom (or top) diode to top (or bottom) IGBT

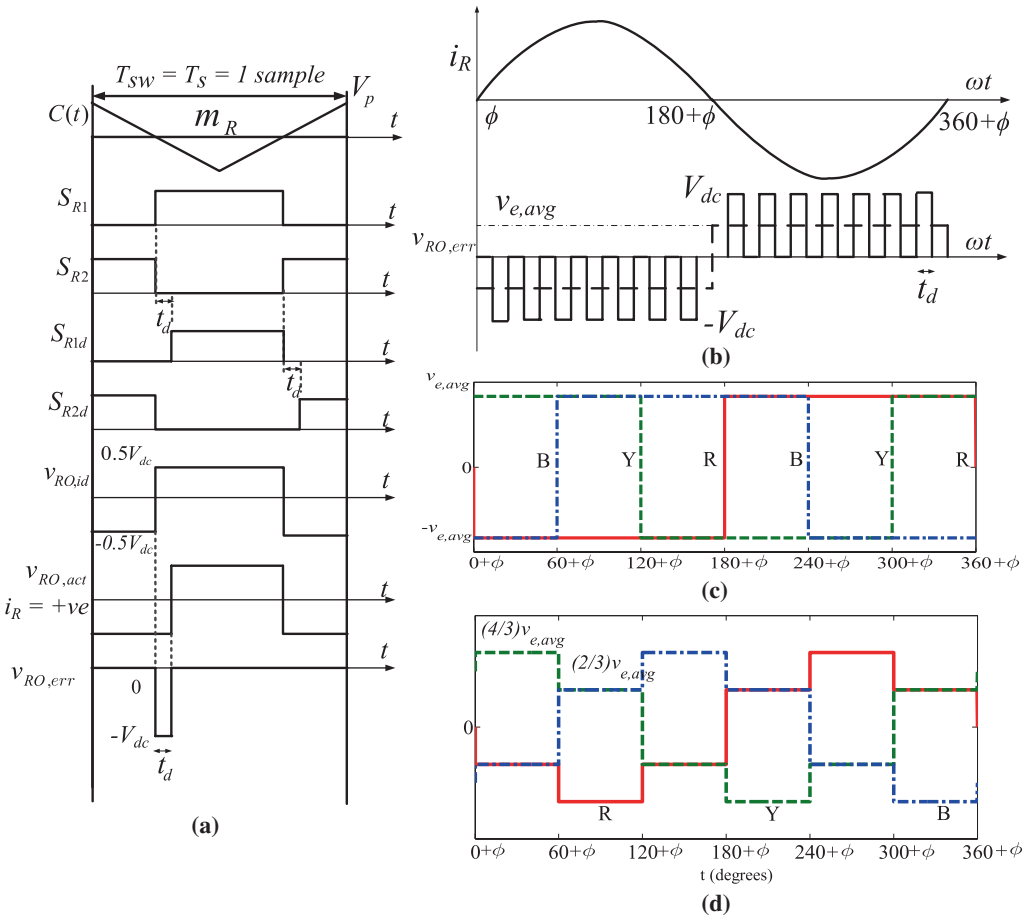


**Figure 3.** (**a**) Dead-time error voltage in a carrier cycle when the line current is positive [6, 16] (**b**) Average dead-time error voltage over a fundamental cycle [6] (**c**) Three-phase average dead-time error voltages at the inverter poles (**d**) Three-phase average line to neutral dead-time error voltages.

transition, the incoming IGBT is delayed by the dead-time duration during which the diode continues to conduct. This results in a deviation from the ideal desired pole voltage, and the instantaneous error voltage $v_{RO,err}$, on account of dead-time is given by (9), where $V_{dc}$ is the dc bus voltage [2, 6, 16].

$$v_{RO,err} = v_{RO,act} - v_{RO,id} = -sign(i_R)V_{dc}. \quad (9)$$

As shown by figure 3(b), the error voltage is seen as a train of negative and positive pulses of width $t_d$ during the positive and negative half cycles of the current respectively. This analysis assumes a continuous pulse width modulation (PWM) scheme such as sine-triangle PWM or conventional space vector modulation. For discontinuous or bus clamping PWM schemes, there are no error voltage pulses (in the pole voltage) in the carrier cycles when the phase is clamped to one of the dc rails [17].

The switching-cycle-average of error voltage is plotted over a fundamental cycle of the current. The average R-phase error voltage ($v_{RO,err,avg}$) is seen to be a square wave of magnitude $v_{e,avg}$, and is out of phase with the load current. The magnitude of the error voltage is expressed as follows:

$$v_{e,avg} = V_{dc} t_d f_{sw} = V_{dc} \frac{t_d}{T_{sw}}. \quad (10)$$

where $f_{sw}$ is the switching frequency, and $T_{sw}$ is the switching cycle [2, 6, 16]. It may be noted that the average error voltage depends only on the dc bus voltage, dead-time duration and the switching frequency. Further, the average error voltage is seen to be independent of the modulating frequency and fundamental voltage. The average Y- and B-phase error voltages are also square waves out of phase with their respective phase currents as shown in figure 3(c). The average error in the three-phase pole voltages is given by

$$\begin{bmatrix} v_{RO,err,avg} \\ v_{YO,err,avg} \\ v_{BO,err,avg} \end{bmatrix} = -v_{e,avg} \begin{bmatrix} sign(i_R) \\ sign(i_Y) \\ sign(i_B) \end{bmatrix}. \quad (11)$$

The average line to neutral error voltages on account of dead-time are shown in figure 3(d). These are given by the following equation:

$$\begin{bmatrix} v_{RN,err,avg} \\ v_{YN,err,avg} \\ v_{BN,err,avg} \end{bmatrix} = -\frac{1}{3} V_{dc} t_d f_{sw} \begin{bmatrix} 2sign(i_R) - sign(i_Y) - sign(i_B) \\ 2sign(i_Y) - sign(i_B) - sign(i_R) \\ 2sign(i_B) - sign(i_R) - sign(i_Y) \end{bmatrix}. \tag{12}$$

Ignoring the ripple in the line current, the three-phase load currents can be represented as follows:

$$\begin{bmatrix} i_R \\ i_Y \\ i_B \end{bmatrix} \approx I_m \begin{bmatrix} \sin(\omega t - \phi) \\ \sin(\omega t - \phi - 120^\circ) \\ \sin(\omega t - \phi - 240^\circ) \end{bmatrix}, \tag{13}$$

where $\phi$ is the power factor angle of the load current. In other words, the polarity of the load current is assumed to be the same as that of its fundamental component. This is quite valid except close to current zero-crossings. Then, the fundamental components of these three-phase error voltages can be expressed as follows:

$$\begin{bmatrix} v_{RN,err,f} \\ v_{YN,err,f} \\ v_{BN,err,f} \end{bmatrix} = -\frac{4}{\pi} V_{dc} t_d f_{sw} \begin{bmatrix} \sin(\omega t - \phi) \\ \sin(\omega t - \phi - 120^\circ) \\ \sin(\omega t - \phi - 240^\circ) \end{bmatrix}. \tag{14}$$

These three-phase fundamental components get transformed into dc components in the dq domain as follows:

$$\begin{bmatrix} v_{qs,err,f} \\ v_{ds,err,f} \end{bmatrix} = -\frac{4}{\pi} V_{dc} t_d f_{sw} \begin{bmatrix} \cos(\phi) \\ \sin(\phi) \end{bmatrix}. \tag{15}$$

Apart from the fundamental component as above, the three-phase error voltages in Eq. (12) also contain non-triplen odd harmonics of order $6n \pm 1$. These harmonics get transformed into harmonics of order $6n$ in the dq reference frame. Hence, the q-axis and d-axis error voltages are periodic over 60°. The variation of these q-axis and d-axis error voltages over a 60° interval is shown in figure 4a and figure 4b, respectively, considering the power factor angle $\phi$ to be 60° (lag). The error voltages shown in figure 4a and figure 4b contain both dc and ripple components. The ripple components in figure 4a and figure 4b are related only to harmonic currents and pulsating torque; these do not contribute to the fundamental current and/or steady average torque. Hence, one could consider only the dc components shown in figure 4a and figure 4b, which correspond to the average q-axis and d-axis error voltages indicated in (15). The corresponding dead-time average error voltage vector can hence be written as follows:

$$\overrightarrow{V}_{s,err,f} = \frac{4}{\pi} V_{dc} \frac{t_d}{T_{sw}} \angle(180^\circ + \phi). \tag{16}$$

Thus, the dead-time error vector can be considered to be a vector of constant magnitude, and out of phase with the current vector. The magnitude of the error vector is fixed, but the phase angle of the error vector $(180^\circ + \phi)$ changes dynamically as the current phase angle $(\phi)$ changes.

## 4. Dynamic model of the induction motor including the effect of dead-time

The space phasor representation of the dead-time effect and the resultant actual inverter output voltage are discussed in this section. The q- and d-axes error voltage components are obtained in terms of the q-axis and d-axis currents, and are incorporated in the model of an inverter fed induction motor.

### 4.1 *Actual inverter output voltage on account of inverter dead-time*

The space-phasor representation of the dead-time effect is shown in figure 5. As seen, the q-axis is aligned with the ideal stator voltage vector $\overrightarrow{V}_{s,id}$, applied to the motor in the absence of dead-time. The actual voltage vector $\overrightarrow{V}_{s,act}$ is the phasor sum of the ideal voltage vector and the dead-time error voltage vector. The load power factor angle is $\phi_{load}$. The apparent power factor angle $\phi$ is the angle between the current vector $\overrightarrow{I}_s$ and the ideal voltage vector $\overrightarrow{V}_{s,id}$. The actual q-axis and d-axis voltage components can be written down in terms of the ideal and error voltage components as shown below:

$$v_{qs} = v_{qs,act} = v_{qs,id} + v_{qs,err,f} \tag{17}$$

$$v_{ds} = v_{ds,act} = v_{ds,id} + v_{ds,err,f}. \tag{18}$$

Using the phasor diagram in figure 5, the q-axis and d-axis error voltage components can be represented in terms of the q-axis and d-axis currents as follows:

$$v_{qs,err,f} = -|\overrightarrow{V}_{s,err,f}| cos\phi = -|\overrightarrow{V}_{s,err,f}| \frac{i_{qs}}{\sqrt{i_{qs}^2 + i_{ds}^2}} \tag{19}$$

$$v_{ds,err,f} = -|\overrightarrow{V}_{s,err,f}| sin\phi = -|\overrightarrow{V}_{s,err,f}| \frac{i_{ds}}{\sqrt{i_{qs}^2 + i_{ds}^2}}. \tag{20}$$

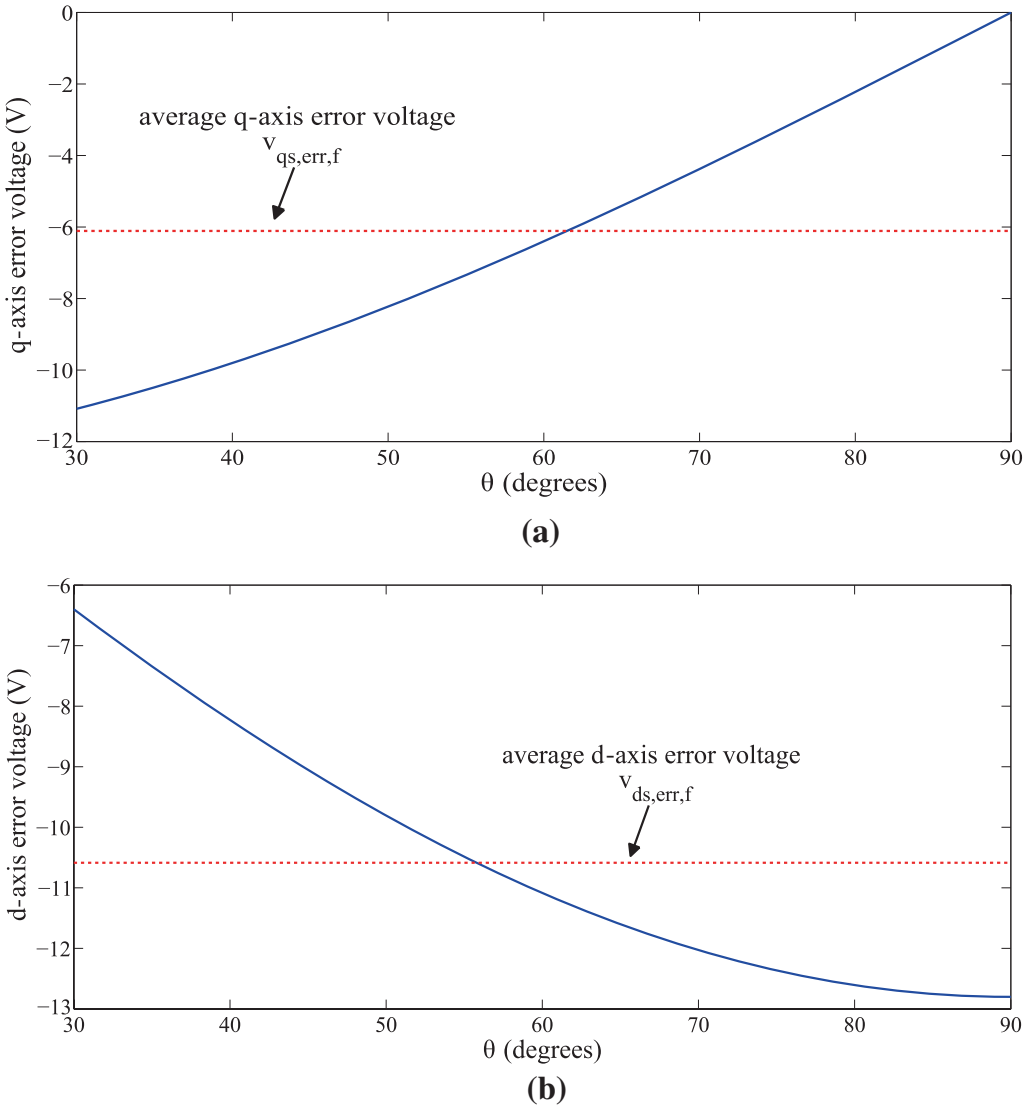


**Figure 4.** (**a**) q-axis error voltage component and (**b**) d-axis error voltage component of the error vector over a 60° interval, considering the power factor angle $\phi$ to be 60° (lag).

Hence, the actual q-axis and d-axis voltages, which are applied at the machine terminals, can be written as shown:

$$v_{qs} = v_{qs,act} = v_{qs,id} - |\vec{V}_{s,err,f}|\frac{i_{qs}}{\sqrt{i_{qs}^2 + i_{ds}^2}} \tag{21}$$

$$v_{ds} = v_{ds,act} = v_{ds,id} - |\vec{V}_{s,err,f}|\frac{i_{ds}}{\sqrt{i_{qs}^2 + i_{ds}^2}}. \tag{22}$$

Here $v_{qs,id}$ and $v_{ds,id}$ are the voltages that would be applied at the load terminals in the absence of dead-time. These are obtained from the ideal sinusoidal modulating signals, scaled by the inverter gain, and transformed to the dq reference frame. The effect of dead-time is included in the dynamic model of the induction machine in the following section.

### 4.2 *Induction motor model including dead-time*

The dynamic model of the induction motor, including dead-time effect in [7] has fluxes and rotor speed as the state variables. This paper develops a dynamic model of induction motor, including effect of dead-time, with the motor currents and electrical speed as the state variables, which is more convenient from the viewpoint of analysis and control. The dynamic model is derived by substituting Eqs. (21) and (22) into (3) and (4), respectively.

$$v_{qs,id} = \left(r_s + L_s\frac{d}{dt} + \frac{|\vec{V}_{s,err,f}|}{\sqrt{i_{qs}^2 + i_{ds}^2}}\right) i_{qs} + \omega_s L_s i_{ds} + L_m\frac{di'_{qr}}{dt} + \omega_s L_m i'_{dr} \tag{23}$$

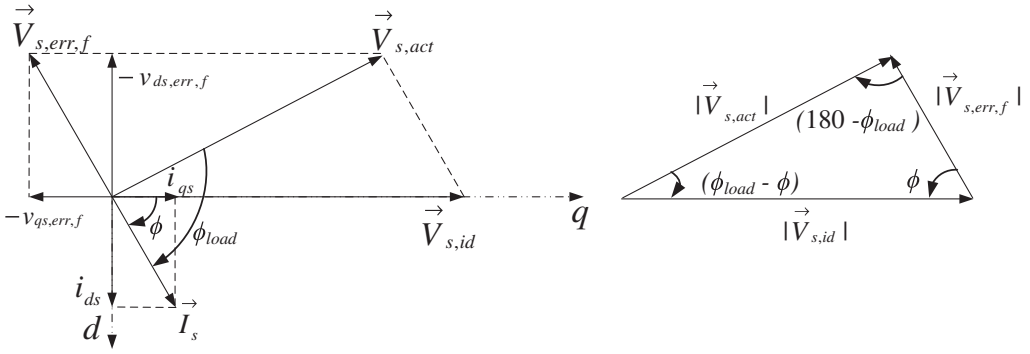


**Figure 5.** Space vector representation of dead-time effect considering the approximate dead-time error vector.

$$v_{ds,id} = -\omega_s L_s i_{qs} + \left( r_s + L_s \frac{d}{dt} + \frac{|\vec{V}_{s,err,f}|}{\sqrt{i_{qs}^2 + i_{ds}^2}} \right) i_{ds} - \omega_s L_m i'_{qr} + L_m \frac{di'_{dr}}{dt} \quad (24)$$

$$v'_{qr} = 0 = L_m \frac{di_{qs}}{dt} + (\omega_s - \omega_r) L_m i_{ds} + \left( r'_r + L'_r \frac{d}{dt} \right) i'_{qr} + (\omega_s - \omega_r) L'_r i'_{dr} \quad (25)$$

$$v'_{dr} = 0 = -(\omega_s - \omega_r) L_m i_{qs} + L_m \frac{di_{ds}}{dt} - (\omega_s - \omega_r) L'_r i'_{qr} + \left( r'_r + L'_r \frac{d}{dt} \right) i'_{dr} \quad (26)$$

$$T_l = \frac{3}{2} \left( \frac{poles}{2} \right) L_m (i_{qs} i'_{dr} - i_{ds} i'_{qr}) - \left( \frac{2}{poles} \right) J \frac{d\omega_r}{dt} - \left( \frac{2}{poles} \right) B \omega_r. \quad (27)$$

The motor is modelled as though it were fed from an ideal VSI; the dead-time error voltage drop is incorporated into the motor model along with the stator resistance drop of the motor in the stator dynamic equations. The dead-time effect is represented by the term $\frac{|\vec{V}_{s,err,f}|}{\sqrt{i_{qs}^2 + i_{ds}^2}}$ which adds to the stator resistance $r_s$ in (23) and (24).

The rotor equations (25) and (26), and mechanical dynamic equation (27) are the same as those of the simple induction motor model, i.e ((5) to (7)). These equations are non-linear since these contain terms which are products of state variables.

The stator voltage equations in the simple dynamic model are linear as seen from (3) and (4). However, incorporation of dead-time effect has rendered these equations non-linear as seen from (23) and (24). Note that the q- and d-axes stator currents appear in the denominator of term representing dead-time effect.

### 4.3 *Simulation study of load change dynamics in a V/F drive*

A 415 V, 4.9 A, 2.2 kW, 1400 RPM, delta-connected induction motor is considered for study. The motor parameters (star/Y equivalent values) are given in table 1. An inverter dead-time of 3.2 μs, dc bus voltage of 600V, and switching frequency of 5kHz are considered to study the impact of dead-time. A sine-triangle modulation scheme is used.

When the motor drive is operating at a modulating frequency of 10Hz, at a V/f ratio of 0.9 pu, the load torque is changed from zero to 0.2 pu rated torque. The simulated q-axis stator current, d-axis stator current, and rotor electrical speed during this transient are shown in figure 6, figure 7, and figure 8, respectively. The simulations are carried out using three different models. The simulations are carried out on a switching-cycle-average basis rather than on an instantaneous basis [16]. The simulated waveforms using the standard induction motor model, neglecting the effect of inverter dead-time (i.e. Eqs. (3) to (7)) are shown in figure 6a, figure 7a, and figure 8a. When three-phase dead-time error voltages as defined in (12) are considered, the corresponding simulated waveforms are as shown in figure 6b, figure 7b and figure 8b. The ripple band is observed in each of these waveforms on account of the harmonic components of order $6n$. Compared to the ripple in the q-axis and d-axis currents (shown in figure 6b and figure 7b, respectively), the ripple in the rotor speed shown in figure 8b is quite low due to inertia of the motor. However, no ripple is observed in any of these quantities, when only the fundamental components of the dead-time error voltages are considered

**Table 1.** Induction motor parameters.

| $r_s$ | $r'_r$ | $L_m$ |
|---|---|---|
| 2.1Ω | 3.6Ω | 0.29 H |
| $L_s = L'_r$ | $J$ | $B$ |
| 0.3H | 0.025 kg m$^2$ | 0 |

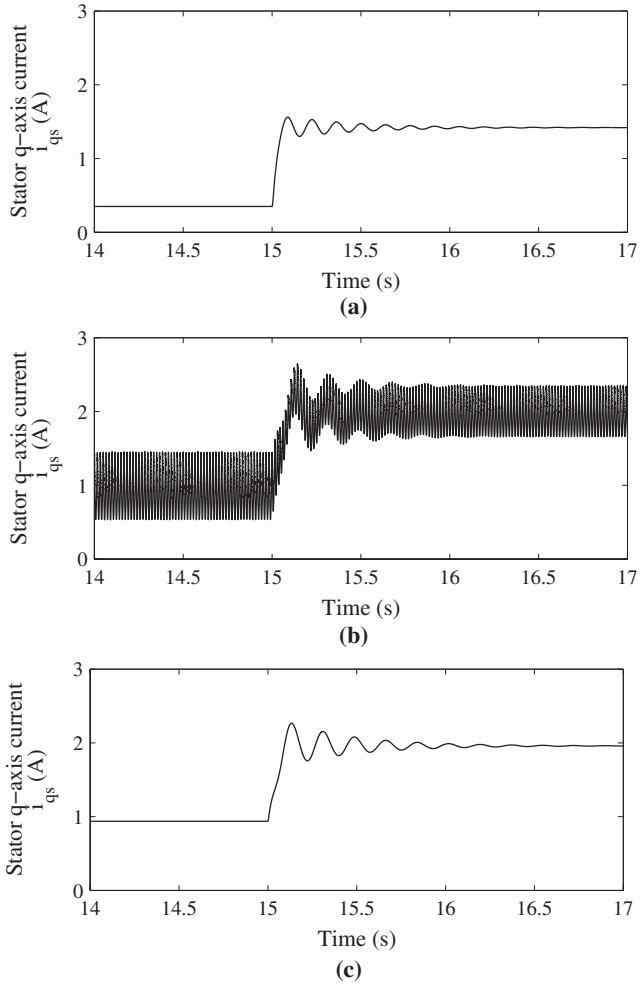


**Figure 6.** Dynamics in the q-axis current for a step change in load torque from no-load to 0.2 pu rated torque. (**a**) without dead-time; (**b**) considering dead-time modelled as a square wave error voltage; (**c**) considering only the fundamental component of the dead-time error voltage.

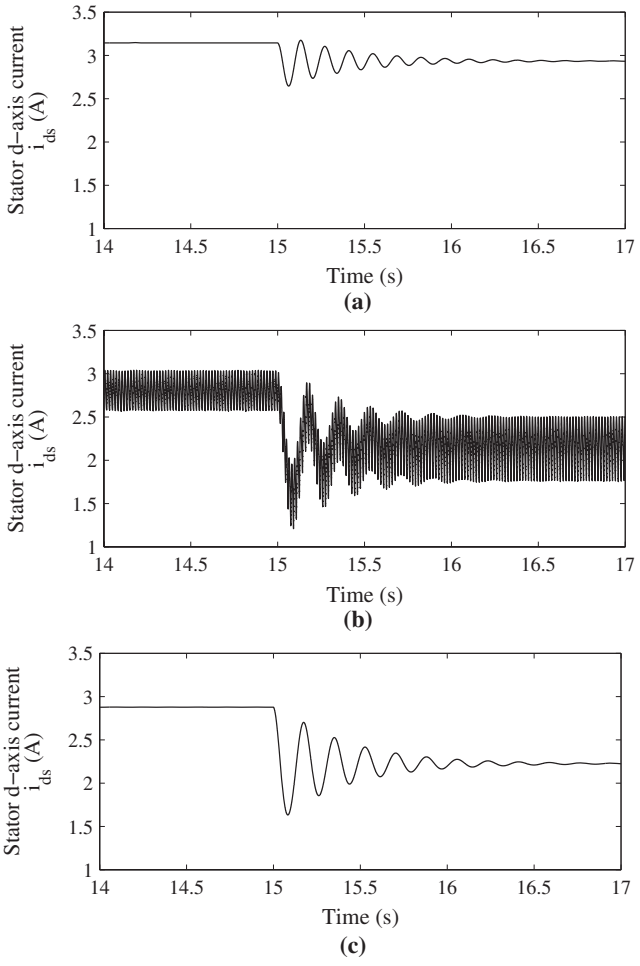


**Figure 7.** Dynamics in the d-axis current for a step change in load torque from no-load to 0.2 pu rated torque. (**a**) without dead-time; (**b**) considering dead-time modelled as a square wave error voltage; (**c**) considering only the fundamental component of the dead-time error voltage.

as shown by (14). These simulation results are shown in figure 6c, figure 7c, and figure 8c. The waveforms in figure 6c, figure 7c, and figure 8c are similar to those in figure 6b, figure 7b and figure 8b, except for the ripple band.

The initial value of q-axis current before the step change in figure 6a, where dead-time is ignored, is lower than that in figure 6c, where the effect of dead-time is considered. The steady-value of the q-axis current, after the transient, is also higher for the case with dead-time. On the other hand the initial value of d-axis current before the step change in figure 7a (dead-time is ignored) is marginally higher than that in figure 7c (dead-time is considered). The steady-value of the d-axis current, after the transient, is significantly lower for the case with dead-time. Thus dead-time has a significant impact on the steady-state operation of the drive. This is studied in detail in the subsequent sections of the paper.

During the transient, oscillations are observed in the q-axis current, d-axis current and the rotor speed. The amplitude of oscillations is increased significantly when dead-time is considered as seen from figure 6, figure 7, and figure 8. These results suggest that the relative stability of the induction motor is somewhat reduced on account of inverter dead-time.

## 5. Steady-state solution of the V/F drive

The steady-state solution of the improved dynamic model of the motor drive ((23) to (27)) is presented in this section. The steady-state solution of the system requires an iterative procedure. The difficulties involved in solving a set of non-linear equations using a typical iterative procedure such as the Newton–Raphson method are outlined. A simplified

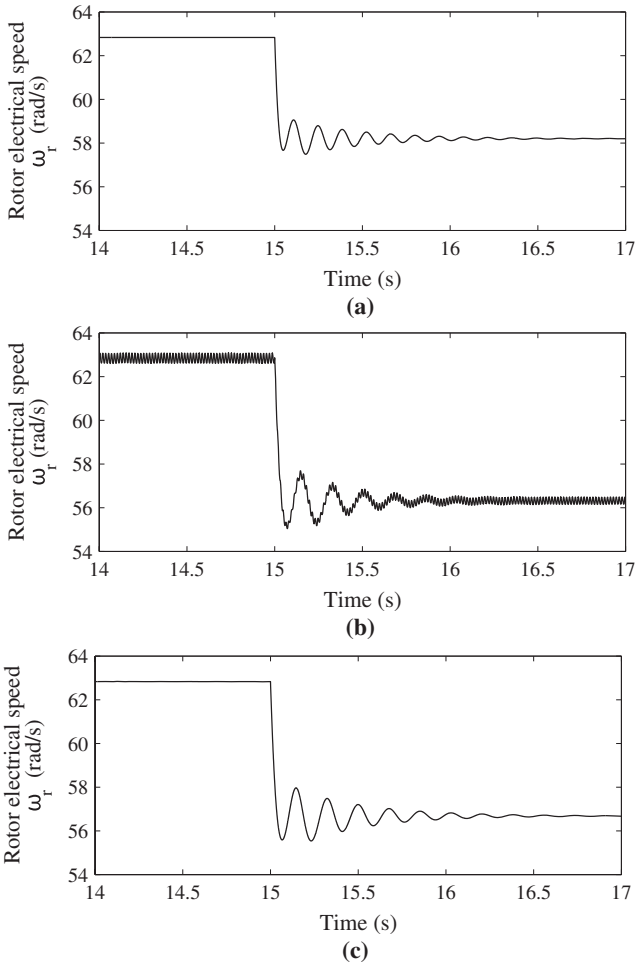


**Figure 8.** Dynamics in the rotor electrical speed for a step change in load torque from no-load to 0.2 pu rated torque. (**a**) without dead-time; (**b**) considering dead-time modelled as a square wave error voltage; (**c**) considering only the fundamental component of the dead-time error voltage.

iterative procedure, invoking the concept of dead-time equivalent resistance, is proposed.

### 5.1 *Steady-state equations of the V/F drive including inverter dead-time*

The steady-state solution is obtained by solving the set of non-linear equations (23)–(27) with the derivative terms set to zero. The system of steady-state equations to be solved is given below.

$$v_{qs,id} = \left( r_s + \frac{|\vec{V}_{s,err,f}|}{\sqrt{i_{qs0}^2 + i_{ds0}^2}} \right) i_{qs0} + \omega_{s0} L_s i_{ds0} + \omega_{s0} L_m i'_{dr0} \tag{28}$$

$$v_{ds,id} = 0 = -\omega_{s0} L_s i_{qs0} + \left( r_s + \frac{|\vec{V}_{s,err,f}|}{\sqrt{i_{qs0}^2 + i_{ds0}^2}} \right) i_{ds0} - \omega_{s0} L_m i'_{qr0} \tag{29}$$

$$v'_{qr} = 0 = (\omega_{s0} - \omega_{r0}) L_m i_{ds0} + (r'_r) i'_{qr0} + (\omega_{s0} - \omega_{r0}) L'_r i'_{dr0} \tag{30}$$

$$v'_{dr} = 0 = -(\omega_{s0} - \omega_{r0}) L_m i_{qs0} - (\omega_{s0} - \omega_{r0}) L'_r i'_{qr0} + (r'_r) i'_{dr0} \tag{31}$$

$$T_l = \frac{3}{2} \left( \frac{poles}{2} \right) L_m (i_{qs0} i'_{dr0} - i_{ds0} i'_{qr0}) - \left( \frac{2}{poles} \right) B \omega_{r0}. \tag{32}$$

### 5.2 *A typical iterative solution method*

The steady-state equations (28)–(32), resulting from the non-linear dynamic equations, are also non-linear. The steady-state solution of this non-linear system with five unknowns (stator and rotor q- and d-axes currents and rotor electrical speed) is not straight-forward, and an iterative procedure is required. A Newton–Raphson method may be attempted.

The five state variables that are to be solved can be written as a column vector as follows:

$$\mathbf{x} = [i_{qs0} \;\; i_{ds0} \;\; i'_{qr0} \;\; i'_{dr0} \;\; \omega_{r0}]^T. \tag{33}$$

Equations (28)–(32) are linearised, and the linearised equations are of the form shown below:

$$\mathbf{u} = \mathbf{J}(\mathbf{\Delta x}). \tag{34}$$

The input vector is given as $\mathbf{u} = [v_{qs,id} \;\; 0 \;\; 0 \;\; 0 \;\; T_l]^T$, and the the Jacobian $\mathbf{J}$ is expressed as follows:

$$\mathbf{J} = \begin{bmatrix} \mathbf{R} & \boldsymbol{\lambda}_{10} \\ \left(\frac{3}{2}\right)\left(\frac{poles}{2}\right)\boldsymbol{\lambda}_{20}^{\mathbf{T}} & \left(\frac{-2}{poles}\right) B \end{bmatrix}, \tag{35}$$

where

$$\mathbf{R} = \begin{bmatrix} r_s + |\vec{V}_{s,err,f}| \left( \frac{i_{ds0}^2}{(i_{qs0}^2 + i_{ds0}^2)^{3/2}} \right) & \omega_{s0} L_s - |\vec{V}_{s,err,f}| \left( \frac{i_{qs0} i_{ds0}}{(i_{qs0}^2 + i_{ds0}^2)^{3/2}} \right) & 0 & \omega_{s0} L_m \\ -\omega_{s0} L_s - |\vec{V}_{s,err,f}| \left( \frac{i_{qs0} i_{ds0}}{(i_{qs0}^2 + i_{ds0}^2)^{3/2}} \right) & r_s + |\vec{V}_{s,err,f}| \left( \frac{i_{qs0}^2}{(i_{qs0}^2 + i_{ds0}^2)^{3/2}} \right) & -\omega_{s0} L_m & 0 \\ 0 & (\omega_{s0} - \omega_{r0}) L_m & r'_r & (\omega_{s0} - \omega_{r0}) L'_r \\ -(\omega_{s0} - \omega_{r0}) L_m & 0 & -(\omega_{s0} - \omega_{r0}) L'_r & r'_r \end{bmatrix}$$

$$\boldsymbol{\lambda}_{10} = [0 \;\; 0 \;\; -(L_m i_{ds0} + L'_r i'_{dr0}) \;\; (L_m i_{qs0} + L'_r i'_{qr0})]^T$$
$$\boldsymbol{\lambda}_{20} = [L_m i'_{dr0} \;\; -L_m i'_{qr0} \;\; -L_m i_{ds0} \;\; L_m i_{qs0}]^T.$$

This Jacobian is evaluated in each iteration, and all the state variables are updated using the inverse of this Jacobian, at the end of each iteration as follows:

$$\mathbf{\Delta x} = \mathbf{J}^{-1}\mathbf{u} \tag{36}$$
$$\mathbf{x_{new}} = \mathbf{x_{old}} + \mathbf{\Delta x}. \tag{37}$$

The iterative process is continued till the solution converges.

The Newton–Raphson method, which is outlined above, requires a good estimate of initial conditions of all the state variables. Also, a $5 \times 5$ Jacobian inverse needs to be evaluated in each iterative step. Further, for non-linear systems, multiple solutions could exist. There could also be problem of non-convergence of the iterative solution. A much simpler procedure is proposed in the following subsections (section 5.3 and section 5.4), which invokes the concept of the dead-time equivalent resistance.

### 5.3 *Analytical expression for the steady-state dead-time equivalent resistance*

The dead-time equivalent resistance ($R_{eq0}$) is defined. A method of approximate evaluation of $R_{eq0}$ is reviewed. Towards precise evaluation of $R_{eq0}$, an analytical expression is derived for the same.

5.3a *Dead-time equivalent resistance*: Consider the phasor diagram shown in figure 5. The dead-time equivalent resistance is defined as the ratio of the magnitude of the dead-time error vector $\overrightarrow{V}_{s,err,f}$ to the magnitude of the steady-state stator current vector $\overrightarrow{I_{s0}}$ as shown below:

$$R_{eq0} = \frac{|\overrightarrow{V}_{s,err,f}|}{\sqrt{i_{qs0}^2 + i_{ds0}^2}} = \frac{|\overrightarrow{V}_{s,err,f}|}{|\overrightarrow{I_{s0}}|}, \tag{38}$$

where the steady-state stator current magnitude can be expressed as

$$|\overrightarrow{I_{s0}}| = \frac{|\overrightarrow{V}_{s,id}|}{|Z_{load} + R_{eq0}|}. \tag{39}$$

Here $|\overrightarrow{V}_{s,id}|$ is the magnitude of the ideal voltage vector and $Z_{load}$ is the motor impedance, which is a function of slip $s$.

5.3b *Approximate value*: As seen from (38) and (39) the dead-time equivalent resistance depends on the load current magnitude which, in turn, depends on the dead-time equivalent resistance. Hence, the solution of the dead-time equivalent resistance is not straight forward. Therefore the following approximation is usually made in the evaluation of load current magnitude [5, 6]:

$$|\overrightarrow{I_{s0}}| \approx \frac{|\overrightarrow{V}_{s,id}|}{|Z_{load}|}. \tag{40}$$

The approximate value of $R_{eq0}$ is calculated based on (38) and (40). The error on account of this approximation is discussed in section 5.5.

5.3c *Actual value*: The stator current magnitude can be expressed in terms of the actual stator voltage vector magnitude $|\overrightarrow{V}_{s,act}|$ as shown below.

$$|\overrightarrow{I_{s0}}| = \frac{|\overrightarrow{V}_{s,act}|}{|Z_{load}|}. \tag{41}$$

Substituting for this current vector magnitude in Eq. (38), the equivalent resistance can be given as follows:

$$R_{eq0} = \frac{|\overrightarrow{V}_{s,err,f}|}{|\overrightarrow{I_{s0}}|} = |Z_{load}|\frac{|\overrightarrow{V}_{s,err,f}|}{|\overrightarrow{V}_{s,act}|}. \tag{42}$$

The vectors $\overrightarrow{V}_{s,err,f}$, $\overrightarrow{V}_{s,id}$, $\overrightarrow{V}_{s,act}$ form a triangle as shown in figure 5, where $\phi_{load}$ is the load power factor angle and $\phi$ is the apparent power factor angle. Applying sine-rule to this triangle,

$$\frac{|\overrightarrow{V}_{s,err,f}|}{\sin(\phi_{load} - \phi)} = \frac{|\overrightarrow{V}_{s,act}|}{\sin(\phi)} = \frac{|\overrightarrow{V}_{s,id}|}{\sin(180^\circ - \phi_{load})}. \tag{43}$$

Based on the above sine-rule the expression for $R_{eq0}$ can be rewritten as

$$R_{eq0} = |Z_{load}|\frac{\sin(\phi_{load} - \phi)}{\sin(\phi)}. \tag{44}$$

Further, the ratio of the fundamental error voltage to the fundamental ideal voltage (i.e. $e$) is defined as

$$e = \frac{|\overrightarrow{V}_{s,err,f}|}{|\overrightarrow{V}_{s,id}|} = \frac{\sin(\phi_{load} - \phi)}{\sin(\phi_{load})} = \frac{\frac{4}{\pi}V_{dc}t_d f_{sw}}{m\frac{V_{dc}}{2}}, \tag{45}$$

where $m$ is the modulation index. Using (44) and (45), the equivalent resistance on account of dead-time is obtained as

$$R_{eq0} = |Z_{load}|(e)\frac{\sin(\phi_{load})}{\sin(\phi)}. \tag{46}$$

Rearranging (45), the apparent power factor angle $\phi$ can be written as

$$\phi = \phi_{load} - \sin^{-1}(esin(\phi_{load})). \tag{47}$$

Substituting for $\phi$ from Eq. (47) into Eq. (46), the dead-time equivalent resistance can be expressed as

$$R_{eq0} = |Z_{load}|\frac{e}{\sqrt{1 - (e^2\sin^2(\phi_{load}))} - (e)\cos(\phi_{load})}. \tag{48}$$

Equations (48) and (45) together constitute an analytic method of evaluating the dead-time equivalent resistance

in steady-state. If the load impedance magnitude and load power factor angle are known, then the equivalent resistance on account of dead-time can be calculated for a given modulation index, dead-time and switching frequency.

### 5.4 *Proposed iterative procedure for steady-state solution*

As mentioned earlier, there are non-linearities in the stator, rotor and torque equations of the induction motor drive including the effect of dead-time. The proposed iterative method is aimed at handling these non-linearities in a simplified manner.

Let an initial value of the rotor speed be assumed. For a given rotor speed (or equivalently, for a given slip), the rotor equations (30) and (31) are now linear. Further $|Z_{load}|$, and $\phi_{load}$, are easily obtained from the induction motor steady-state equivalent circuit at the given slip. Hence, the dead-time equivalent resistance $R_{eq0}$ can be evaluated using (45) and (48). This can be used to replace the non-linear term $\frac{|\overrightarrow{V}_{s,err,f}|}{\sqrt{i_{qs0}^2+i_{ds0}^2}}$ in Eqs. (28) and (29). Now, the resulting stator equations are also linear. Hence, the four motor currents ($i_{qs}$, $i_{ds}$, $i'_{qr}$, $i_{dr}\prime$) can be obtained by solving the set of four linear equations (i.e two stator equations and two rotor equations).

The load torque for the given rotor speed and motor currents are calculated using (32). The difference between the calculated load torque and the actual load torque is the torque error. Assuming the torque-slip characteristics to be linear, the torque error can be converted into an equivalent speed error. The speed error is then used to update the rotor speed. The updated rotor speed is used for solving the motor currents in each iteration by handling the non-linearities as discussed above. The iterative process is continued till the torque error (or speed error) is small.

The steps to obtain the steady solution are outlined as follows:

1. Calculate the ratio $e$ of the fundamental error voltage magnitude $|\overrightarrow{V}_{s,err,f}|$ to the ideal voltage magnitude $|\overrightarrow{V}_{s,id}|$ from Eq. (45).
2. Assume an initial value of the rotor electrical speed $\omega_{r0}$, say $\omega_{r0} = \omega_{s0}$.
3. From the synchronous speed $\omega_{s0}$ and the rotor electrical speed $\omega_{r0}$, calculate the slip ($s$) of the motor.
4. Calculate the load impedance magnitude $|Z_{load}|$ and phase angle $\phi_{load}$ at the given slip ($s$) using the steady-state equivalent circuit of the induction motor.
5. Calculate $R_{eq0}$ using (48) with the values of $e$, $|Z_{load}|$ and $\phi_{load}$ obtained as above.
6. Substitute for the non-linear resistance term in (28) and (29) with $R_{eq0}$.
7. Evaluate the stator and rotor q- and d-axes currents by simultaneous solution of the two stator equations and two rotor equations, which are now linear.
8. Substitute for the above currents into Eq. (32), and calculate the estimated load torque $T_{l,calc}$.
9. Find the error $T_{l,err}$ between the input load torque $T_l$ and the estimated load torque $T_{l,calc}$ as shown:

$$T_{l,err} = T_l - T_{l,calc}.$$

10. If the torque error is less than the tolerance, then stop the iteration; the solution is obtained.
11. If the error is greater than the tolerance, then use the torque error to calculate the new rotor speed as shown:

$$\omega_{r0,new} = \omega_{r0,old} - k_T(T_{l,err})$$

where $k_T$ is the ratio of the rated electrical angular slip speed to the rated torque.

12. Use the new rotor electrical speed and repeat from step 3.

Observe that initial guess is required only for one state variable, i.e. rotor electrical speed, as against initial values of all state variables in a typical Newton–Raphson solution scheme. The initial value for the rotor electrical speed is taken to be the synchronous speed. This is a good estimate at light-loads, and is reasonable under loaded condition also. Further, the steady-state torque-speed characteristics of the motor could also be considered to make the initial guess of rotor speed under loaded conditions.

### 5.5 *Evaluation of dead-time equivalent resistance*

The dead-time equivalent resistance can be evaluated analytically using Eqs. (45) and (48). This equivalent resistance depends on the load impedance $Z_{load}$ which, in turn, depends on the operating slip ($s$). At no-load, the slip $s = 0$, and $Z_{load}$ is known directly. However, under loaded condition, the slip and load impedance need to be obtained through the iterative process described in section 5.4.

The value of $R_{eq0}$ is determined at different fundamental frequencies and V/f ratios under no-load as discussed above. The motor parameters are shown in table 1. The inverter has a dead-time of 3.2 μs, a dc bus voltage of 600V and is switched at a frequency of 5kHz. The results are shown plotted in figure 9 (solid lines). The corresponding approximate values of $R_{eq0}$, calculated using (38) and (40), are also shown plotted in the same figure (dashed lines). As seen the approximate method of evaluating $R_{eq0}$ leads to significant error at low modulation frequencies.

Similarly $R_{eq0}$ is evaluated at different modulation frequencies and at different values of load torque, considering a V/f ratio of 0.9 pu. The actual and approximate values of dead-time equivalent resistance are shown plotted in figure 10 as solid and dashed lines, respectively. Once again the approximate method of evaluation is found to result in significant error at low modulation frequencies.

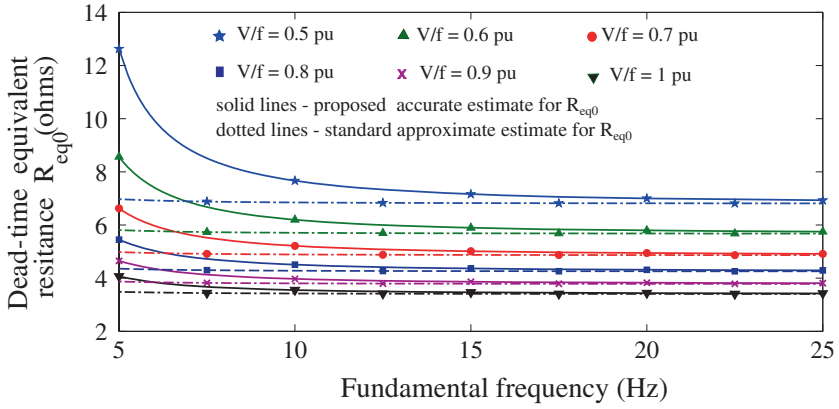


**Figure 9.** Dead-time equivalent resistance $R_{eq0}$ at different fundamental frequencies and V/f ratios under no-load.

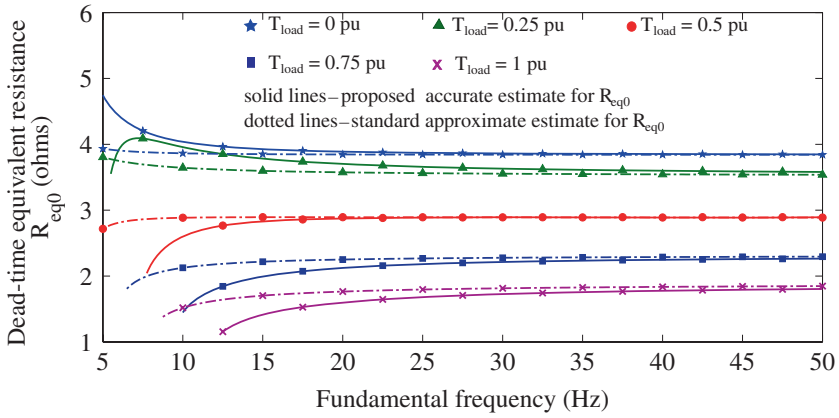


**Figure 10.** Dead-time equivalent resistance $R_{eq0}$ at different fundamental frequencies and load torques, considering a V/f ratio of 0.9 pu.

### 5.6 *Steady solution under different loads – solutions based on proposed method and simulation results*

The same motor as in section 5.5 is considered. The inverter has a dc bus voltage of 600 V, and is switched at a frequency of 5kHz with sine-triangle PWM. Time domain simulations are carried out using the dynamic models of the inverter-fed motor, both considering and ignoring dead-time.

For an inverter dead-time of 3.2 µs the simulated steady-state waveforms of $i_{qs}$, $i_{ds}$, $i'_{qr}$, $i'_{dr}$, $\omega_r$ are shown in figure 11a to figure 11e, respectively, for a fundamental frequency of 10 Hz, and at no-load. The simulated stator and rotor currents and the rotor electrical speed, neglecting dead-time, are also shown in the same figures; these state variables are perfect dc quantities at steady-state as seen from figure 11. However, with a dead-time of 3.2 µs, a ripple component is observed, in addition to the dc component in the waveforms. The dc component or average value in the dq frame is representative of the fundamental frequency component in the RYB frame, as mentioned earlier in section 3. The ripple is indicative of the low-frequency harmonics introduced on account of dead-time, as discussed earlier in section 3. The average q-axis current is found to increase on account of dead-time as seen from figure 11a, while the average d-axis current reduces due to dead-time effect, as brought out by figure 11b (the rated motor current of 6.93A (peak) equals 1 pu).

Simulations are performed at 0 pu, 0.25 pu and 0.5 pu of rated torque for the same fundamental frequency of 10 Hz, switching frequency of 5 kHz and dead-time of 3.2 µs. The average values of $i_{qs}$, $i_{ds}$, $i'_{qr}$, $i'_{dr}$ and $\omega_r$ obtained through simulation are tabulated in table 2. The average values of the simulated currents and rotor speed match closely with the solutions based on the proposed iterative procedure (described in section 5.4), which are also shown in the same table 2.

Similarly, table 3 and table 4 present the steady-state values of the state variables based on the iterative procedure, considering a different dead-time of 1.5 µs, and without dead-time, respectively. The corresponding simulated average values of currents and rotor speed are also tabulated.

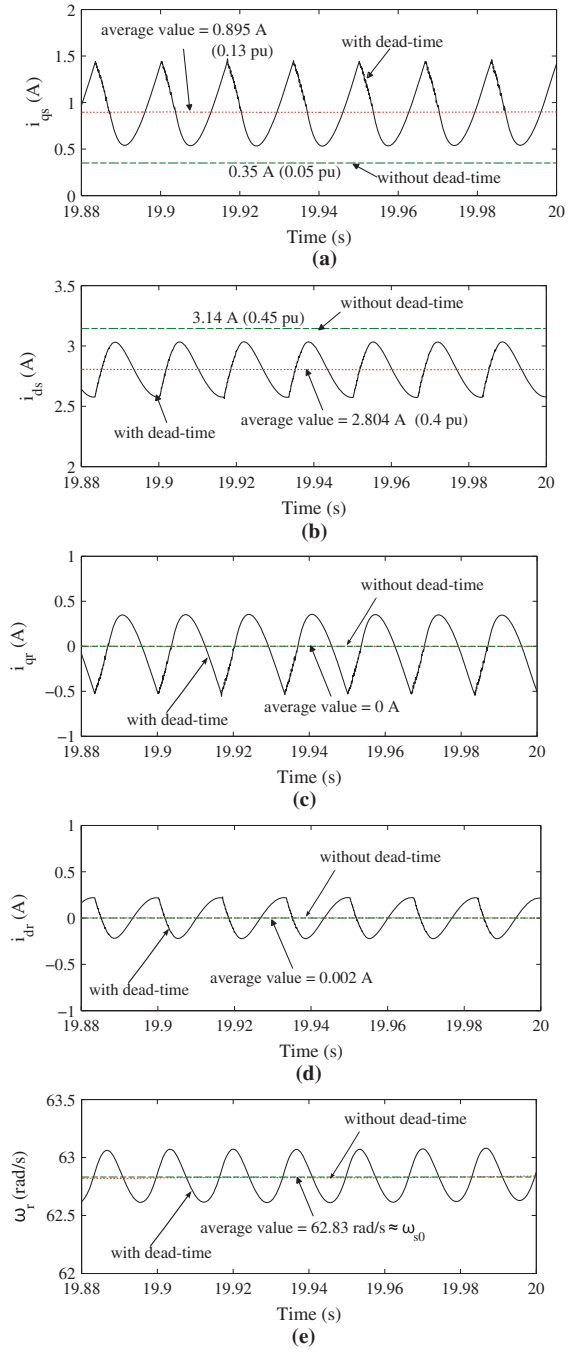


**Figure 11.** Simulated steady-state waveforms of the system state variables, at a fundamental frequency of 10 Hz, and at no-load. (**a**) q-axis stator current; (**b**) d-axis stator current; (**c**) q-axis rotor current; (**d**) d-axis rotor current; (**e**) rotor electrical speed. Each waveform consists of a dc value that relates to the fundamental component and ripple components of the form $6n\omega_s$, on account of the low-frequency harmonic components arising from the dead-time effect.

For a given value of dead-time, as the load torque increases, the q-axis current increases, while the d-axis current and rotor speed decrease. For a given load-torque, it is observed that with an increase in the dead-time duration, the q-axis current increases, while the d-axis current reduces; the rotor electrical speed reduces as well.

## 6. Steady-state solution of the V/F drive including the effect of inverter dead-time under no-load condition

It may be recalled from section 1 that dead-time could cause the induction motor drive to be unstable from a small-signal perspective [6, 7, 10, 13], particularly close to no-load. Small-signal stability analysis for predicting such light-load instability requires the knowledge of the steady-state operating conditions under no-load. This section focuses on the impact of dead-time on the steady-state operating point of the drive under no-load.

### 6.1 *Closed form expression for the no-load solution*

With the load torque being zero, and neglecting frictional torque (i.e. B = 0), the slip speed is approximately zero and the steady-state rotor electrical speed is the same as the synchronous speed.

$$\omega_{r0} = \omega_{s0}. \tag{49}$$

The steady-state rotor currents are also zero under no-load.

$$i'_{qr0} = i'_{dr0} = 0. \tag{50}$$

With the slip speed being zero, the impedance offered by the induction motor is effectively its no-load impedance (i.e. stator resistance in series with the stator reactance). Hence $|Z_{load}|$ and $\phi_{load}$ are expressed as follows:

$$|Z_{load}| = \sqrt{(r_s)^2 + (\omega_s L_s)^2} \tag{51}$$

$$\phi_{load} = \tan^{-1}\left(\frac{\omega_s L_s}{r_s}\right). \tag{52}$$

The dead-time equivalent resistance $R_{eq0}$ is evaluated using Eq. (45) and (48). Replacing the non-linear stator resistance term in (28) and (29), by $R_{eq0}$, and the rotor currents being zero, the stator equations simplify as follows:

$$v_{qs,id} = m\frac{V_{dc}}{2} = (r_s + R_{eq0})i_{qs0} + \omega_s L_s i_{ds0} \tag{53}$$

$$v_{ds,id} = 0 = -\omega_s L_s i_{qs0} + (r_s + R_{eq0})i_{ds0}. \tag{54}$$

Equations (53) and (54) can be solved to yield the stator currents. An analytic closed form solution (non-iterative) is possible and a simplified solution is obtained using the idea of the dead-time equivalent resistance. Hence, the complete steady-state analytic solution of the induction motor drive

**Table 2.** Comparison of the solutions based on the proposed method, and simulated solutions at different loads considering $f_1 = 10$ Hz, $f_{sw} = 5$ kHz and $t_d = 3.2$ µs.

| Load torque (in p.u) | $i_{qs0}$ (A) | | $i_{ds0}$ (A) | | $i'_{qr0}$ (A) | | $i'_{dr0}$ (A) | | $\omega_{ro}$ (rad/s) | |
|---|---|---|---|---|---|---|---|---|---|---|
| | Proposed iterative | Simulated | Proposed iterative | Simulated | Proposed iterative | Simulated | Proposed iterative | Simulated | Proposed iterative | Simulated |
| 0 | 0.94 | 0.90 | 2.88 | 2.80 | 0 | 0 | 0 | 0 | 62.83 | 62.83 |
| 0.25 | 2.27 | 2.25 | 2.09 | 2.07 | −1.66 | −1.71 | 0.37 | 0.34 | 54.54 | 54.07 |
| 0.5 | 4.35 | 4.37 | 1.78 | 1.87 | −4.04 | −4.12 | 0.33 | 0.22 | 39.18 | 38.35 |

**Table 3.** Comparison of the solutions based on the proposed method, and simulated solutions at different loads considering $f_1 = 10$ Hz, $f_{sw} = 5$ kHz and $t_d = 1.5$ µs.

| Load torque (in p.u) | $i_{qs0}$ (A) | | $i_{ds0}$ (A) | | $i'_{qr0}$ (A) | | $i'_{dr0}$ (A) | | $\omega_{ro}$ (rad/s) | |
|---|---|---|---|---|---|---|---|---|---|---|
| | Proposed iterative | Simulated | Proposed iterative | Simulated | Proposed iterative | Simulated | Proposed iterative | Simulated | Proposed iterative | Simulated |
| 0 | 0.63 | 0.63 | 3.05 | 3.02 | 0 | 0 | 0 | 0 | 62.83 | 62.83 |
| 0.25 | 1.98 | 1.98 | 2.55 | 2.54 | −1.51 | −1.53 | 0.23 | 0.22 | 56.11 | 55.99 |
| 0.5 | 3.69 | 3.69 | 2.29 | 2.29 | −3.39 | −3.41 | 0.25 | 0.22 | 46.19 | 46.0 |

**Table 4.** Comparison of the solutions based on the proposed method, and simulated solutions at different loads considering $f_1 = 10$ Hz, $f_{sw} = 5$ kHz and without inverter dead-time.

| Load torque (in p.u) | $i_{qs0}$ (A) | | $i_{ds0}$ (A) | | $i'_{qr0}$ (A) | | $i'_{dr0}$ (A) | | $\omega_{ro}$ (rad/s) | |
|---|---|---|---|---|---|---|---|---|---|---|
| | Proposed iterative | Simulated | Proposed iterative | Simulated | Proposed iterative | Simulated | Proposed iterative | Simulated | Proposed iterative | Simulated |
| 0 | 0.35 | 0.35 | 3.14 | 3.14 | 0 | 0 | 0 | 0 | 62.83 | 62.83 |
| 0.25 | 1.7 | 1.7 | 2.89 | 2.89 | −1.43 | −1.43 | 0.11 | 0.11 | 56.92 | 56.92 |
| 0.5 | 3.25 | 3.25 | 2.72 | 2.72 | −3.05 | −3.05 | 0.1 | 0.1 | 49.46 | 49.46 |

under no-load, including the effect of dead-time is given as follows:

$$\begin{bmatrix} i_{qs0} \\ i_{ds0} \\ i'_{qr0} \\ i'_{dr0} \\ \omega_{r0} \end{bmatrix} = \begin{bmatrix} v_{qs,id} \frac{(r_s+R_{eq0})}{(r_s+R_{eq0})^2+(\omega_s L_s)^2} \\ v_{qs,id} \frac{(\omega_s L_s)}{(r_s+R_{eq0})^2+(\omega_s L_s)^2} \\ 0 \\ 0 \\ \omega_{s0} \end{bmatrix}. \quad (55)$$

The q-axis and d-axis current components can also be equivalently represented by magnitude and phase of the stator current vector. The magnitude of the current vector $|\overrightarrow{I_s}|$, and the angle $\phi$ that this vector makes with the q-axis or the ideal voltage vector are calculated as follows:

$$|\overrightarrow{I_s}| = \sqrt{i_{qs0}^2 + i_{ds0}^2} \quad (56)$$

$$\phi = \tan^{-1}\left(\frac{i_{ds0}}{i_{qs0}}\right). \quad (57)$$

The analytical solution presented here is validated through simulations in the following section.

## 6.2 *Analytical and simulated steady-state no-load stator current*

The q-axis and d-axis stator currents are evaluated analytically using Eq. (55). Further, the current vector magnitude and phase angle are evaluated from these q-axis and d-axis currents using (56) and (57). The induction motor parameters given in table 1, and an inverter dc bus voltage of 600 V are considered for the various plots presented in this subsection.

The analytically evaluated $i_{qso}$ and $i_{dso}$ at no-load are plotted against fundamental frequencies ranging between 5 Hz and 50 Hz in figure 12a and figure 12b, respectively. These currents are evaluated at different switching frequencies of 2.5 kHz, 3.75 kHz, 5 kHz and 6.25 kHz, considering a dead-time of 3.2 µs. Figure 12a and figure 12b also show the q-axis and d-axis currents, respectively, ignoring the effect of dead-time. The stator current magnitude and angle ($\phi$) are shown plotted in figure 12c and figure 12d, respectively.

Under no-load, the induction motor offers a predominantly inductive impedance. Neglecting the stator resistance drop, the stator current magnitude ($|\overrightarrow{I_s}|$), and apparent

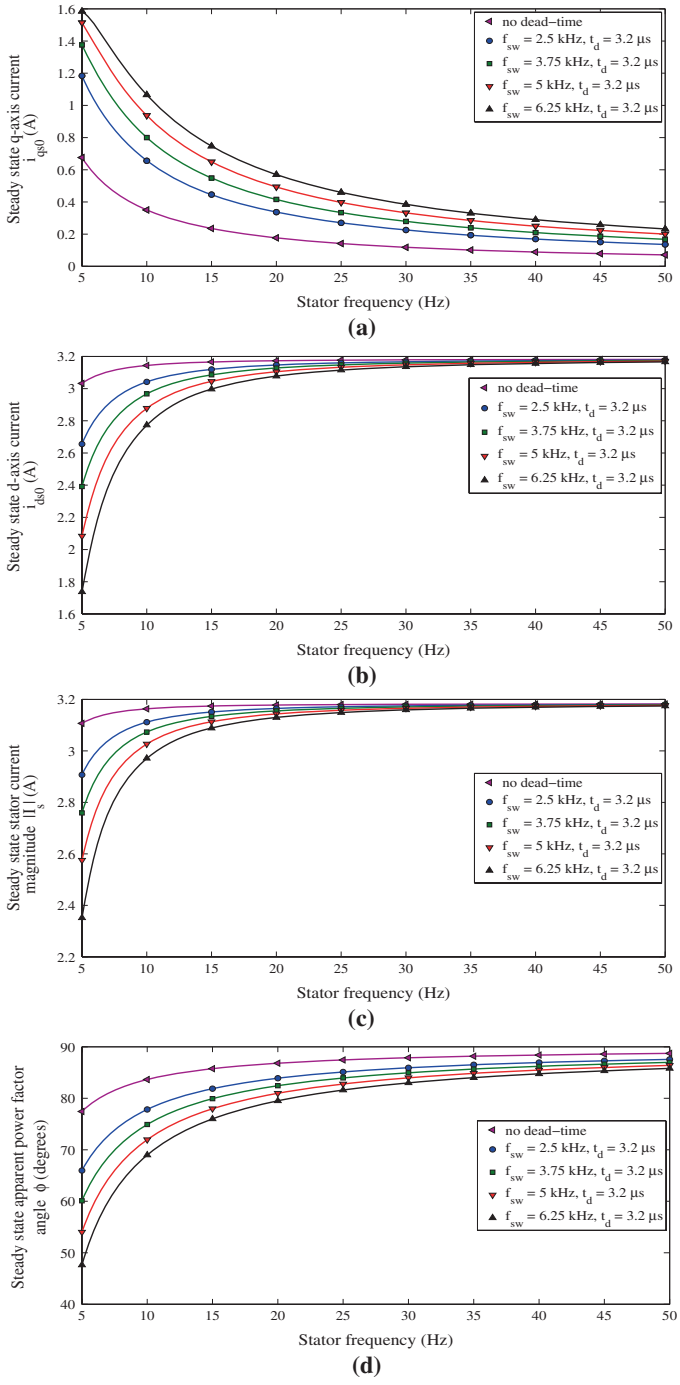


**Figure 12.** Analytically evaluated steady-state values of (**a**) q-axis stator current; (**b**) d-axis stator current; (**c**) stator current magnitude and (**d**) apparent power factor angle ($\phi$) against fundamental stator frequency in a constant V/f drive under no-load, at different switching frequencies, on account of an inverter dead-time of 3.2 µs.

power factor angle ($\phi$) are ideally expected to be nearly constant, across the range of fundamental frequencies, and at different switching frequencies. However, as the fundamental frequency decreases, there is a decrease in the magnitude of the stator current, and apparent power factor angle ($\phi$), even without dead-time. There is a decrease in the d-axis stator current also, indicating a reduction in the motor flux. This behaviour is attributed to the stator resistance drop of the motor, which cannot be neglected in comparison to the inductive impedance, at lower speeds.

This drop in the stator current magnitude and that in the apparent power factor angle at lower speed are further accentuated by the effect of dead-time. As the switching frequency increases, the stator current magnitude and the

apparent power factor angle decrease. The dead-time effect is such that an apparent equivalent resistance adds to the stator resistance. This equivalent resistance increases as the inverter switching frequency increases. Hence, a relatively more resistive behaviour is observed from the waveforms in figure 12, as the switching frequency increases.

Time domain simulations are also performed to verify the analytically evaluated currents. The average values of the simulated currents are considered as discussed earlier in section 5.6. The simulated stator q-axis and d-axis no-load currents, the stator current magnitude and apparent power factor angle are shown plotted against fundamental

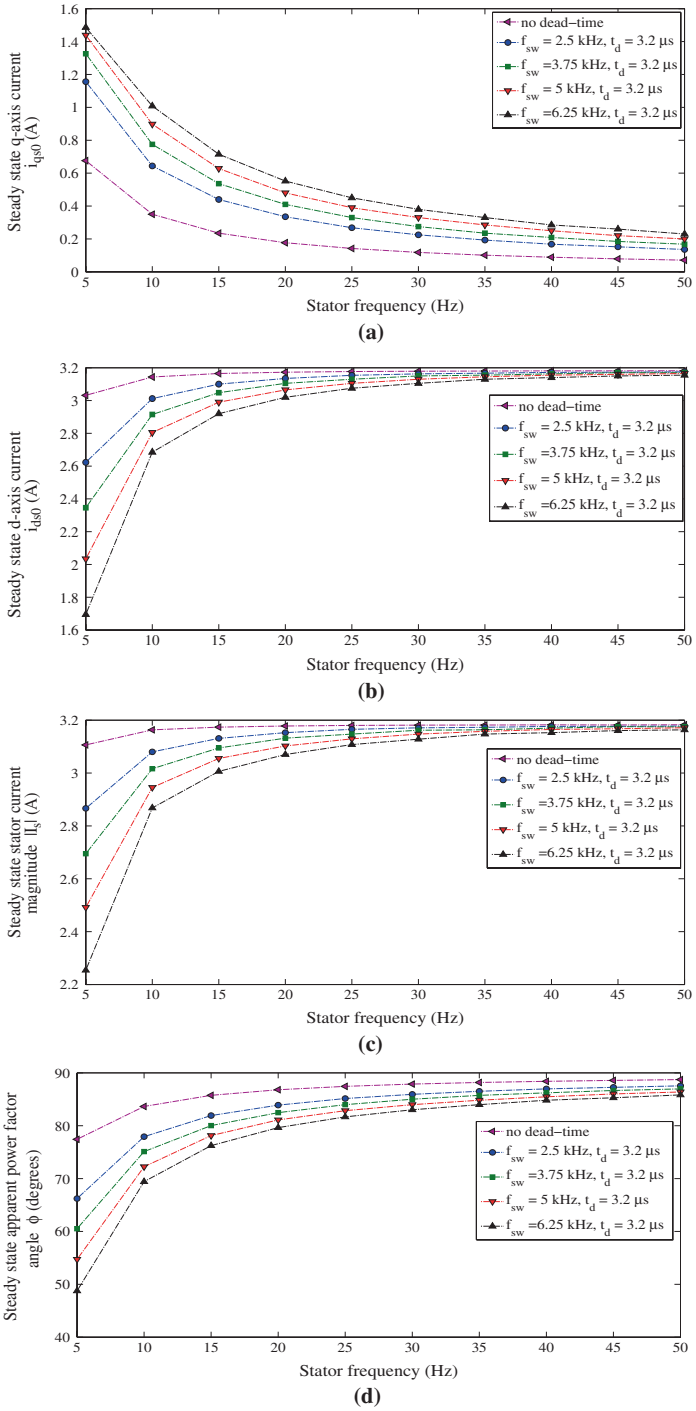


**Figure 13.** Simulated steady-state values of (**a**) q-axis stator current; (**b**) d-axis stator current; (**c**) stator current magnitude and (**d**) apparent power factor angle ($\phi$) against fundamental stator frequency in a constant V/f drive under no-load, at different switching frequencies, on account of an inverter dead-time of 3.2 µs.

frequency in figure 13. The plots are presented for different switching frequencies, considering a dead-time of 3.2 μs. The analytically evaluated currents in figure 12 match closely with the simulated values in figure 13.

The analytically evaluated steady-state stator currents, considering a smaller dead-time of 1.5 μs, are shown plotted in figure 14. Further, the accentuation of the drop in the stator current magnitude and that in the apparent power factor angle with increased switching frequency are verified, for this value of dead-time also. The simulated values of the stator currents, considering a dead-time of 1.5 μs, are shown plotted in figure 15. These are in close agreement with the analytical estimates in figure 14. The variations in the steady-state stator currents on account of the inverter dead-time are verified experimentally in the following section.

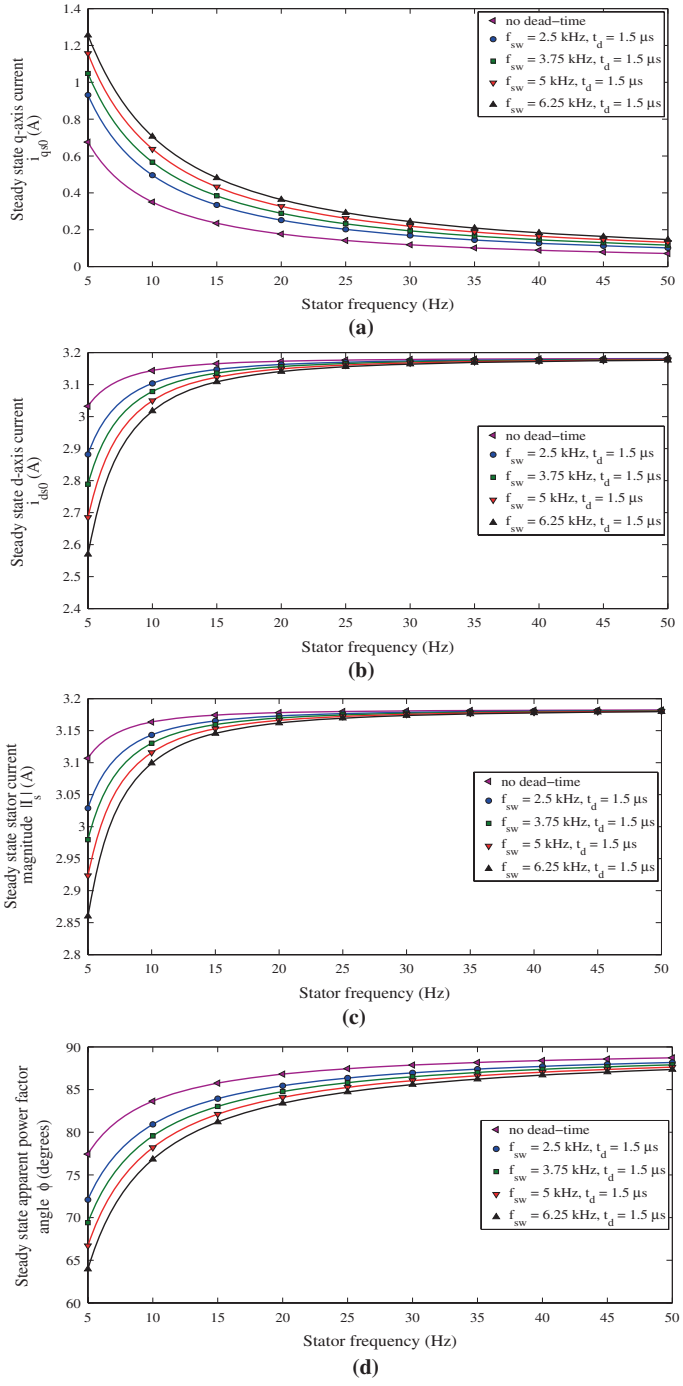


**Figure 14.** Analytically evaluated steady-state values of (**a**) q-axis stator current; (**b**) d-axis stator current; (**c**) stator current magnitude and (**d**) apparent power factor angle ($\phi$) against fundamental stator frequency in a constant V/f drive under no-load, at different switching frequencies, on account of an inverter dead-time of 1.5 μs.

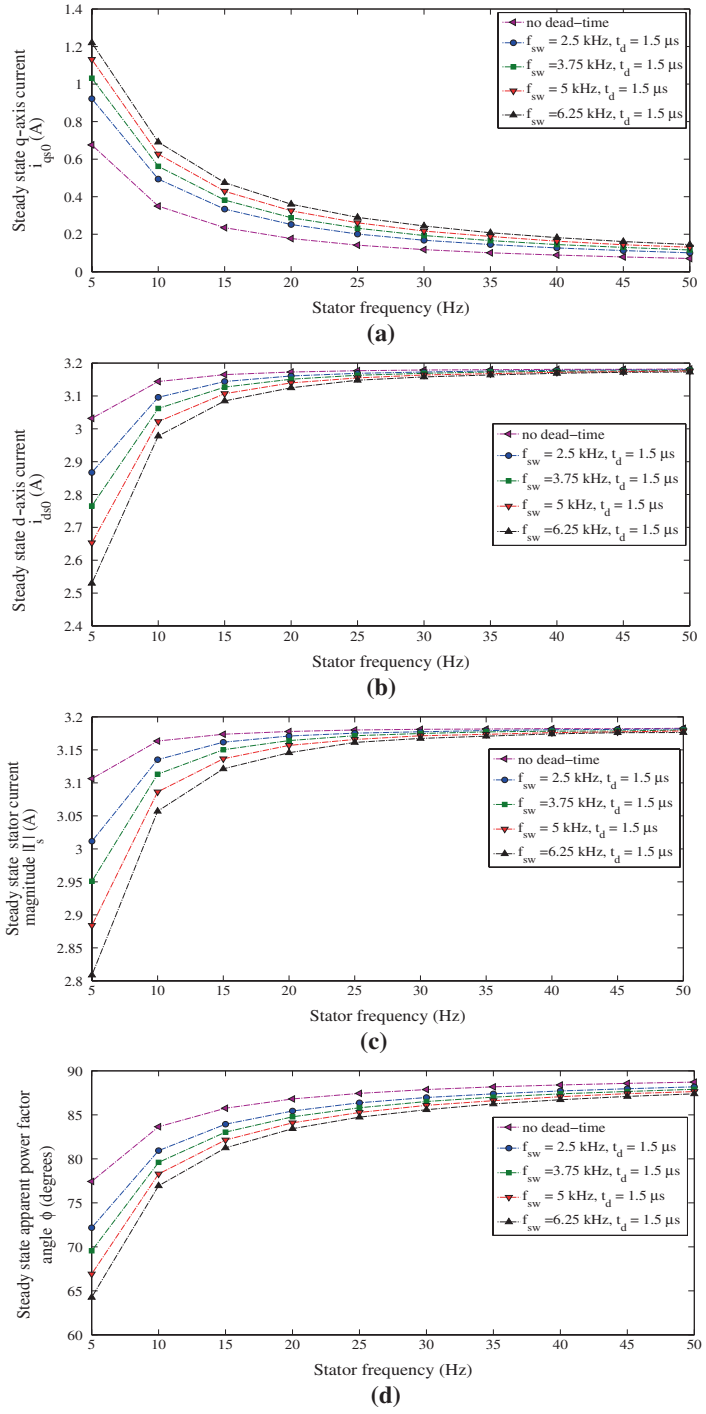


**Figure 15.** Simulated steady-state values of (**a**) q-axis stator current; (**b**) d-axis stator current; (**c**) stator current magnitude and (**d**) apparent power factor angle ($\phi$) against fundamental stator frequency in a constant V/f drive under no-load, at different switching frequencies, on account of an inverter dead-time of 1.5 µs.

## 7. Experimental verification of the impact of inverter dead-time on the no-load steady-state stator currents of the V/F drive

The experimental set-up consists of a 2-level voltage source inverter, feeding a 2.2 kW induction motor. The motor details are the same as given in table 1 and section 5.6. The front-end of the VSI is a diode bridge rectifier that is fed from the ac mains through an autotransformer. The inverter dc bus voltage is maintained at 600 V. Experiments are performed with this practical voltage source inverter, having a dead-time of 3.2 µs. The measured steady-state q-axis and

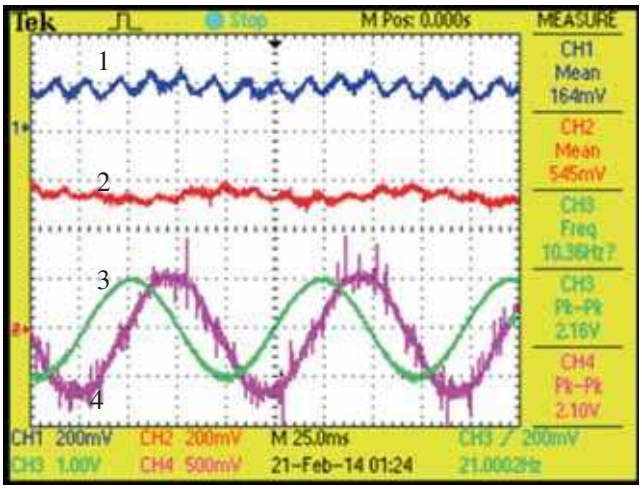


**Figure 16.** Measured q-axis, d-axis and R-phase stator currents under no-load, at a fundamental frequency of 10 Hz, with an inverter dead-time of 3.2 μs, and switching frequency of 2.5 kHz . Trace 1: q-axis current (1 A/div), Trace 2: d-axis current (1 A/div), Trace 3: Ideal R-phase fundamental stator voltage (60 V/div), Trace 4: R-phase current (2.5 A/div).

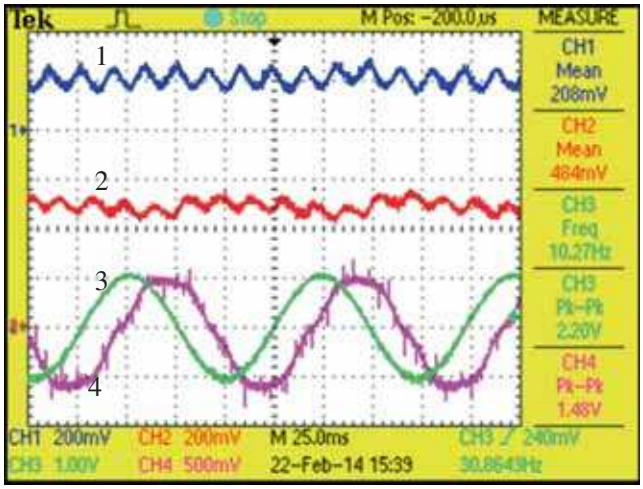


**Figure 18.** Measured q-axis, d-axis and R-phase stator currents under no-load, at a fundamental frequency of 10 Hz, with an inverter dead-time of 3.2 μs, and switching frequency of 5 kHz . Trace 1: q-axis current (1 A/div), Trace 2: d-axis current (1 A/div), Trace 3: Ideal R-phase fundamental stator voltage (60 V/div), Trace 4: R-phase current (2.5 A/div).

d-axis stator currents under no-load are shown in figure 16, at a fundamental frequency of 10 Hz and a switching frequency of 2.5 kHz. The R-phase modulating signal, which is representative of the ideal stator voltage, and the R-phase stator current are also shown in the figure. The current is observed to be lagging the voltage by about 72°.

Experimentally measured waveforms at the same fundamental frequency of 10 Hz, but at different switching frequencies of 3.75 kHz, 5 kHz and 6.25 kHz, are shown in figure 17, figure 18 and figure 19, respectively. As the switching frequency increases from 2.5 kHz to 6.25 kHz, the d-axis current reduces from about 2.7A to 2.2A, indicating reduction in flux. The angle, by which the current lags the ideal modulating signal, changes from about 72° at 2.5 kHz to about 60° at 6.25 kHz. This ascertains the fact that the dead-time equivalent resistance increases with switching frequency.

The average q-axis and d-axis currents at these different switching frequencies are measured at different fundamental frequencies ranging from 5 Hz to 50 Hz in steps of

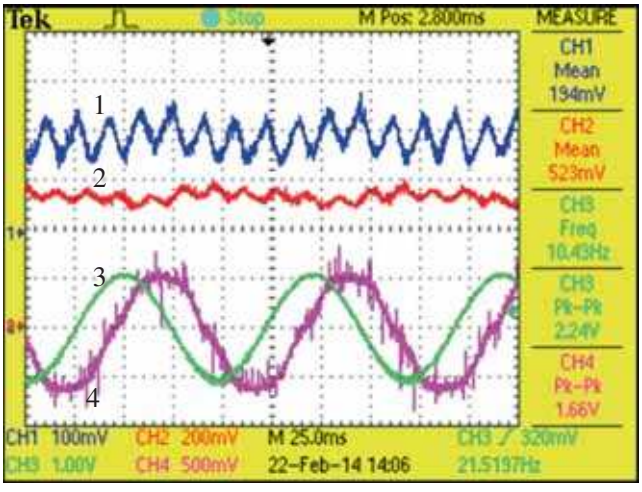


**Figure 17.** Measured q-axis, d-axis and R-phase stator currents under no-load, at a fundamental frequency of 10 Hz, with an inverter dead-time of 3.2 μs, and switching frequency of 3.75 kHz. Trace 1: q-axis current (0.5 A/div), Trace 2: d-axis current (1 A/div), Trace 3: Ideal R-phase fundamental stator voltage (60 V/div), Trace 4: R-phase current (2.5 A/div).

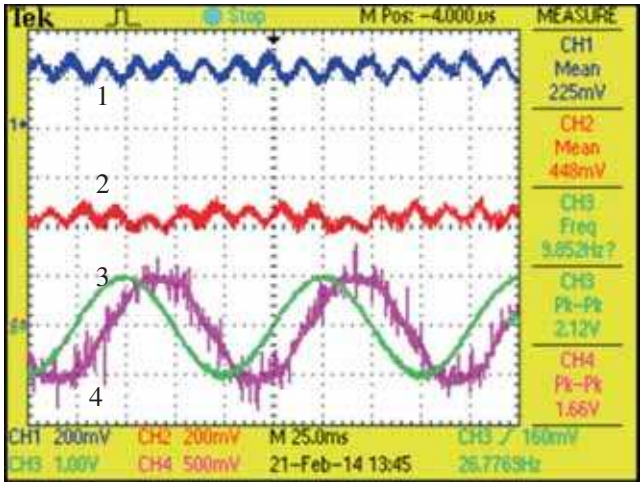


**Figure 19.** Measured q-axis, d-axis and R-phase stator currents under no-load, at a fundamental frequency of 10 Hz, with an inverter dead-time of 3.2 μs, and switching frequency of 6.25 kHz. Trace 1: q-axis current (1 A/div), Trace 2: d-axis current (1 A/div), Trace 3: Ideal R-phase fundamental stator voltage (60 V/div), Trace 4: R-phase current (2.5 A/div).

5 Hz. The measured variations in the q-axis and d-axis currents, and the corresponding variations in the stator current magnitude and apparent power factor angle $\phi$ are plotted in figure 20. The nature of variations is similar to the analytical predictions and the simulation results. The d-axis current, stator current magnitude and apparent power factor angle are found to decrease with decrease in the fundamental frequency. At any given fundamental frequency, the d-axis current, stator current magnitude and power factor angle decrease with increase in switching frequency. This is in conformation with the theoretical predictions. The nature of the variation of the no-load stator currents, on account of inverter dead-time, has been verified experimentally.

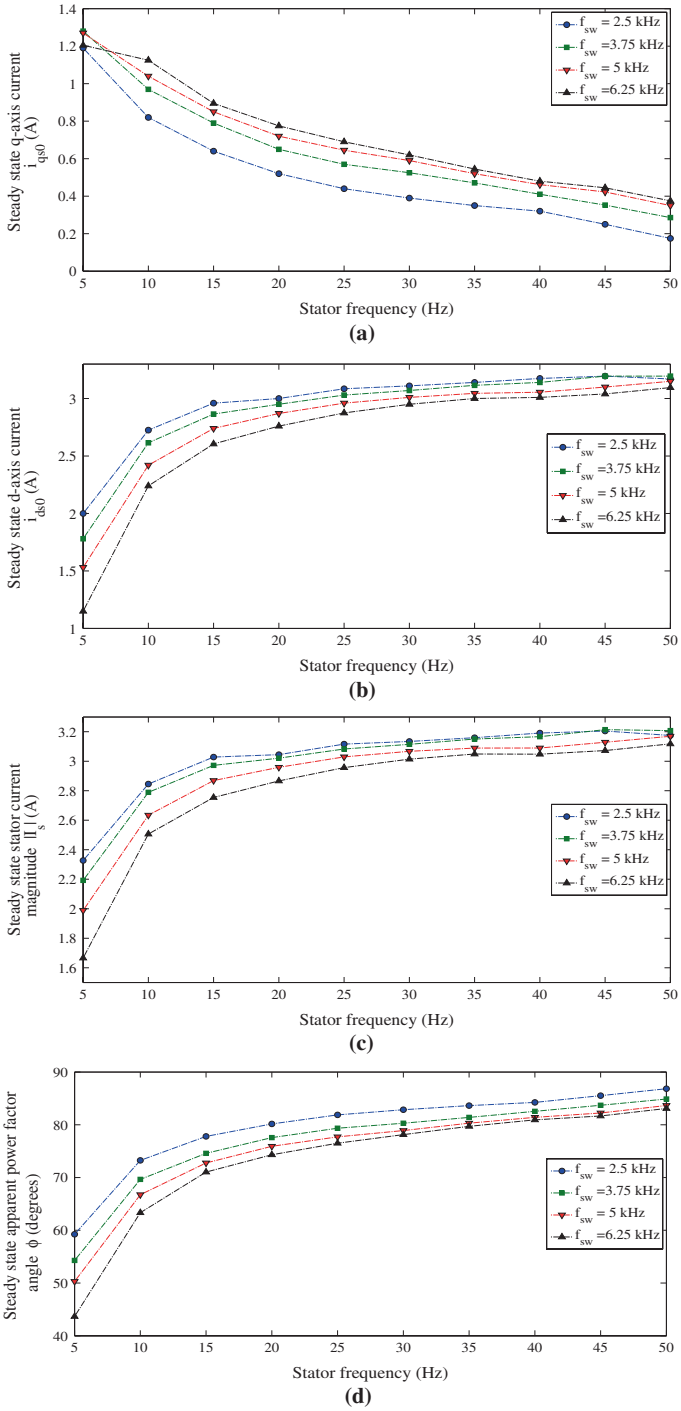


**Figure 20.** Measured steady-state values of (**a**) q-axis stator current; (**b**) d-axis stator current; (**c**) stator current magnitude and (**d**) apparent power factor angle ($\phi$) against fundamental stator frequency in a constant V/f drive under no-load, at different switching frequencies, on account of an inverter dead-time of 3.2 μs.

## 8. Conclusion

The inverter dead-time is integral to the safety of any voltage source inverter, and is universal to any inverter fed-induction motor drive. To study the impact of dead-time on an open-loop induction motor drive, this paper presents the systematic derivation of a dynamic model of an inverter fed induction motor drive, including the effect of inverter dead-time, in the synchronous dq reference frame. Simulation results demonstrating load change transients in the open-loop induction motor drive are illustrated in the paper, both considering and ignoring inverter dead-time. Amplitude of oscillations in the q-axis and d-axis current components, and rotor speed are increased on account of dead-time. Simulation results also show significant variation in the steady-state operating condition on account of dead-time.

To study the steady-state behaviour of the system in detail, the dynamic model is used to derive a steady-state model, which is found to be non-linear. Hence, determination of the steady-state operating point of a motor drive, having significant dead-time, requires an iterative procedure. This iterative procedure is simplified by invoking the concept of dead-time equivalent resistance. The non-linear term on account of dead-time is modelled as an equivalent variable resistance ($R_{eq0}$) that appears in series with the stator resistance. A rigorous treatment of dead-time equivalent resistance is presented in this paper. An analytical expression is proposed for this steady-state equivalent dead-time resistance in terms of the dead-time, switching frequency, modulation index, and load impedance. This expression for $R_{eq0}$ is used in the evaluation of the steady-state solution of the drive through a simplified iterative procedure. Further, this leads to simple closed form expressions for the state variables at steady-state under no-load. The analytical results, thus obtained using the equivalent resistance approach, are validated through time-domain simulations and actual measurements on a 2.2 kW induction motor drive.

## References


[1] Murai Y, Watanabe T and Iwasaki H 1987 Waveform distortion and correction circuit for pwm inverters with switching lag-times. *IEEE Trans. Ind. Appl.* 5: 881–886

[2] Jeong S G and Park M H 1991 The analysis and compensation of dead-time effects in pwm inverters. *IEEE Trans. Ind. Electron.* 38(2): 108–114

[3] Choi J W and Sul S K 1996 Inverter output voltage synthesis using novel dead time compensation. *IEEE Trans. Power Electron.* 11(2): 221–227

[4] Mao X, Ayyanar R and Jain A K 2011 Dead time effect in two-level space vector pwm voltage source inverters with large current ripple. In: *Proceedings of IEEE Applied Power Electronics Conference and Exposition.* 679–684

[5] Colby R S, Simlot A K and Hallouda M A 1990 Simplified model and corrective measures for induction motor instability caused by pwm inverter blanking time. *Conference Record IEEE Power Electronics Specialists Conference (PESC).* 678–683

[6] Guha A, Tripathi A and Narayanan G 2013 Experimental study on dead-time induced oscillations in a 100-kw open-loop induction motor drive. In: *Proceedings of National Power Electronics Conference NPEC 2013, IIT Kanpur.* 1–6

[7] Vasic V, Marcetic D, Oros D and Kulic F 2009 Prediction of local instabilities caused by inverter dead time in ac drive. In: *Proceedings of European Conference Power Electronics and Applications (EPE).* 1–9

[8] Ahmed S, Shen Z, Mattavelli P, Boroyevich D, Jaksic M, Karimi K and Fu J 2011 Small-signal model of a voltage source inverter (vsi) considering the dead-time effect and space vector modulation types. In: *Proceedings of IEEE Applied Power Electronics Conference and Exposition.* 685–690

[9] Nelson R H, Lipo T A and Krause P C 1969 Stability analysis of a symmetrical induction machine. *IEEE Transactions Power Apparatus and Systems* 11: 1710–1717

[10] Ueda R, Sonoda T and Takata S 1989 Experimental results and their simplified analysis on instability problems in pwm inverter induction motor drives. *IEEE Trans. Ind. Appl.* 25(1): 86–95

[11] Koga K, Ueda R and Sonoda T 1988 Stability problem in induction motor drive system. *Conference Record of IEEE Industry Applications Society Annual Meeting.* 129–136

[12] Ueda R, Sonoda T, Koga K and Ichikawa M 1992 Stability analysis in induction motor driven by a v/f controlled general-purpose inverter. *IEEE Trans. Ind. Appl.* 28(2): 472–481

[13] Guha A and Narayanan G 2014 Small-signal stability analysis of an open-loop induction motor drive including the effect of inverter dead-time. *In: Proceedings of IEEE International Conference on Power Electronics, Drives and Energy Systerms, (IEEE PEDES)*: 1–6

[14] Guha A and Narayanan G 2015 Small-signal stability analysis of an open-loop induction motor drive including the effect of inverter dead-time. *IEEE Trans. Ind Appl.* 1–9

[15] Krishnan R 2001 *Electric motor drives – modelling, analysis and control*. Pearson Education

[16] Guha A and Narayanan G 2013 Average modelling of a voltage source inverter with dead-time in a synchronous reference frame. In: *Proceedings of IEEE Innovative Smart Grid Technologies-Asia (ISGT Asia).* 1–6

[17] Roy T, Hari V S S P K and Narayanan G 2013 Study on the Effect of Dead Time and its Compensation for Bus-Clamping PWM Techniques. In: *Proceedings of National Power Electronics Conference NPEC 2013, IIT Kanpur.* 1–6